ANISOTROPIC STRESS-STRAIN BEHAVIOR AT SMALL STRAINS OF CLAY BY TRIAXIAL AND BENDER ELEMENT TESTS

Satoshi Yamashita[1], Member, JGS, Tomohito Hori[2], Student Member, JGS, and Teruyuki Suzuki[3], Member, JGS

ABSTRACT: In this study, to examine the effect of the fabric anisotropy on elastic moduli (shear and Young's moduli), the bender element, cyclic and monotonic triaxial tests were performed on reconstituted clay specimens with different fabric characteristics. The specimens with the angle between the axial direction of the triaxial specimen and the bedding direction of 0 and 90 degrees were cut from the pre-consolidated clay block. These specimens were isotropically consolidated under several kinds of confining pressures. The shear wave velocities in three different directions (VH, HH, HV-wave) were measured by bender element tests, and the stiffness under wide ranges of strain levels up to failure were measured by cyclic and monotonic triaxial tests. Test results showed that; 1) the shear modulus obtained from the shear wave for propagating and vibrating horizontal to the bedding plane is higher than the others two kinds of moduli, 2) the horizontal Young's modulus at small strain is also higher than the vertical one, 3) the anisotropy of the elastic modulus of clay is larger than that with sand, but becomes lower with the increase in strain level and consolidation stress.

INTRODUCTION

The shear and Young's moduli at small strain, G_{max} and E_{max}, called "quasi-elastic modulus", are known to be close to the maximum value under given stress/strain conditions, and they are independent of shearing rate, type of loading (monotonic or cyclic), number of cycles, etc. To assess the in-situ small strain stiffness, laboratory tests on samples retrieved from the site or in-situ tests have been performed. In in-situ seismic surveys, the down-hole or suspension technique measures V_{vh},

[1] Associate Professor, Kitami Institute of Technology, 165 Koen-cho, Kitami, 090-8507, Japan, yamast@mail.kitami-it.ac.jp
[2] Graduate Student, Kitami Institute of Technology, 165 Koen-cho, Kitami, 090-8507, Japan
[3] Professor, Kitami Institute of Technology, 165 Koen-cho, Kitami, 090-8507, Japan

whereas V_{hh} or V_{hv} is measured by the cross-hole technique. Note that the first and second subscripts for V denote the directions of shear wave propagation and polarization, respectively. On the other hand, in laboratory tests, one technique that has been widely adopted in the last decade is the propagation of seismic waves by means of piezoelectric transducers, called simply "bender element", housed in a triaxial apparatus (e.g. Dyvik and Madshus 1985). In this method, the shear wave velocity propagated vertically, V_{vh}, is commonly measured.

The above techniques are based on the following relationship between the velocity of the seismic body wave and the shear modulus of an isotropic homogeneous elastic medium;

$$G_{max} = \rho V_S^2 \tag{1}$$

where G_{max} is the maximum shear modulus; ρ is the total mass density of the medium; and V_S is the shear wave velocity.

If the soil ground is homogeneous and under isotropic stress conditions, the shear wave velocity, V_{vh}, should be equal to V_{hh} and V_{hv}. However, the shear wave velocities are different from the propagating directions, since the in-situ stress conditions may be mostly anisotropic, and the in-situ subsoil has an anisotropic fabric.

In the literature, Butcher and Powell (1995) and Hight et al. (1997) reported that in-situ shear wave velocities measured by cross-hole and down-hole techniques are different based on the propagating directions, and they are different based on the kinds of soils (sandy or clayey soils). In addition, Yimsiri and Soga (2002) reported that clays are generally more anisotropic than sands in terms of small-stain stiffness and fabric conditions in the laboratory test.

In this paper, to clarify the effect of the propagating and vibrating directions of shear wave relative to the bedding plane on a clay specimen's small-strain stiffness, bender element tests, and monotonic and cyclic triaxial tests were performed on reconstituted clay specimens. The shear wave velocities from three different directions (VH, HH, HV-wave) and the stiffness under a wide range of strain levels up to failure were measured by bender element and triaxial tests.

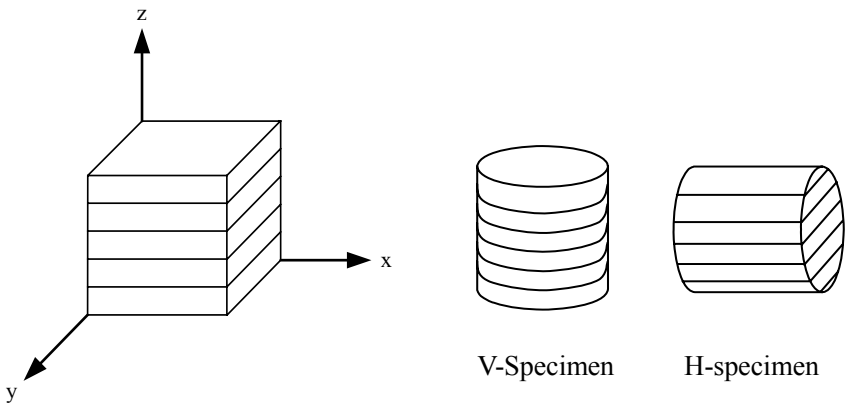

FIG. 1. Illustration of a Cross-Anisotropic Material, V-Specimen and H-Specimen

STRESS STRAIN RELATIONSHIP

Cross Anisotropic Model

When elasticity is cross-anisotropic and if the anisotropy is symmetrical about the vertical axis, as shown in Fig. 1, we obtain the following stress-strain equation:

$$\begin{bmatrix} \delta\varepsilon_{xx} \\ \delta\varepsilon_{yy} \\ \delta\varepsilon_{zz} \\ \delta\varepsilon_{yz} \\ \delta\varepsilon_{zx} \\ \delta\varepsilon_{xy} \end{bmatrix} = \begin{bmatrix} \frac{1}{E_h} & \frac{-\nu_{hh}}{E_h} & \frac{-\nu_{vh}}{E_v} & 0 & 0 & 0 \\ \frac{-\nu_{hh}}{E_h} & \frac{1}{E_h} & \frac{-\nu_{vh}}{E_v} & 0 & 0 & 0 \\ \frac{-\nu_{hv}}{E_h} & \frac{-\nu_{hv}}{E_h} & \frac{1}{E_v} & 0 & 0 & 0 \\ 0 & 0 & 0 & \frac{1}{G_{hv}} & 0 & 0 \\ 0 & 0 & 0 & 0 & \frac{1}{G_{vh}} & 0 \\ 0 & 0 & 0 & 0 & 0 & \frac{1}{G_{hh}} \end{bmatrix} \begin{bmatrix} \delta\sigma_{xx}' \\ \delta\sigma_{yy}' \\ \delta\sigma_{zz}' \\ \delta\sigma_{yz}' \\ \delta\sigma_{zx}' \\ \delta\sigma_{xy}' \end{bmatrix} \tag{2}$$

where x and y-axes are horizontal and z-axis is vertical; E_v and E_h are the vertical and horizontal Young's moduli; ν_{vh}, ν_{hh} and ν_{hv} are the Poisson's Ratios; G_{vh}, G_{hh} and G_{hv} are the shear moduli.

From Eq.(2), the following stress-strain relations are obtained;

$$\delta\varepsilon_{xx} = \frac{1}{E_h}\delta\sigma_{xx}' - \frac{\nu_{hh}}{E_h}\delta\sigma_{yy}' - \frac{\nu_{vh}}{E_v}\delta\sigma_{zz}' \tag{3}$$

$$\delta\varepsilon_{yy} = -\frac{\nu_{hh}}{E_h}\delta\sigma_{xx}' + \frac{1}{E_h}\delta\sigma_{yy}' - \frac{\nu_{vh}}{E_v}\delta\sigma_{zz}' \tag{4}$$

$$\delta\varepsilon_{zz} = -\frac{\nu_{hv}}{E_h}\delta\sigma_{xx}' - \frac{\nu_{hv}}{E_h}\delta\sigma_{yy}' + \frac{1}{E_v}\delta\sigma_{zz}' \tag{5}$$

From the symmetry of the matrix and the isotropic property in the horizontal plane, Eqs. (6) and (7) are obtained;

$$\frac{\nu_{vh}}{E_v} = \frac{\nu_{hv}}{E_h} \tag{6}$$

$$G_{hh} = \frac{E_h}{2(1+\nu_{hh})} \tag{7}$$

Drained and Undrained Triaxial Tests under Constant Lateral Pressure on V-Specimens

When the loading direction is z-direction, $\delta\sigma_{xx}'$ and $\delta\sigma_{yy}'$ are zero, in the drained triaxial test on the V-specimen, which was vertically cut from the block sample as shown in Fig. 1. Thus, from Eq.(5), the following relation is obtained;

$$E_v = \frac{\delta\sigma_{zz}'}{\delta\varepsilon_{zz}} = \frac{\delta q}{\delta\varepsilon_{zz}} \tag{8}$$

where q is the deviator stress.

On the other hand, in the undrained test, since $\delta\sigma_{xx}'$ is equal to $\delta\sigma_{yy}'$, substitution of Eq.(6) into Eq.(5) leads to;

$$\delta\varepsilon_{zz} = -\frac{\nu_{vh}}{E_v}\delta\sigma_{xx}' - \frac{\nu_{vh}}{E_v}\delta\sigma_{yy}' + \frac{1}{E_v}\delta\sigma_{zz}' \tag{9a}$$

$$E_v = \frac{\delta\sigma_{zz}' - 2\nu_{vh}\delta\sigma_{xx}'}{\delta\varepsilon_{zz}} \tag{9b}$$

Under undrained conditions, the volumetric strain $\delta\varepsilon_{vol}$ is zero. $\delta\varepsilon_{xx}$ is equal to $\delta\varepsilon_{yy}$, when the loading direction is the z-direction.

$$\delta\varepsilon_{vol} = \delta\varepsilon_{xx} + \delta\varepsilon_{yy} + \delta\varepsilon_{zz} = 0 \tag{10a}$$

$$\delta\varepsilon_{xx} = -\frac{\delta\varepsilon_{zz}}{2} \tag{10b}$$

$$\nu_{vh} = -\frac{\delta\varepsilon_{xx}}{\delta\varepsilon_{zz}} = 0.5 \tag{11}$$

Substitution of Eq.(11) into Eq.(9b) leads to the Young's modulus for the vertical direction under undrained conditions, $(E_v)_u$.

$$(E_v)_u = \frac{\delta\sigma_{zz}' - \delta\sigma_{xx}'}{\delta\varepsilon_{zz}} = \frac{\delta q}{\delta\varepsilon_{zz}} \tag{12}$$

Accordingly, the vertical Young's modulus is directly measured from the increment of axial stress and strain from drained or undrained triaxial tests under constant lateral pressure on V-specimens.

Drained and Undrained Triaxial Tests under Constant Lateral Pressure on H-Specimens

When the loading direction is x-direction, $\delta\sigma_{yy}'$ and $\delta\sigma_{zz}'$ are zero, in the drained triaxial test on the H-specimen, which was horizontally cut from the block sample as shown in Fig. 1. Thus, from Eq.(3), the following relation is obtained;

$$E_h = \frac{\delta\sigma_{xx}'}{\delta\varepsilon_{xx}} = \frac{\delta q}{\delta\varepsilon_{xx}} \tag{13}$$

On the other hand, in the undrained test, since $\delta\sigma_{yy}'$ is equal to $\delta\sigma_{zz}'$, substitution of Eq.(6) into Eq.(3) leads to:

$$\delta\varepsilon_{xx} = \frac{1}{E_h}\delta\sigma_{xx}' - \frac{\nu_{hh}}{E_h}\delta\sigma_{yy}' - \frac{\nu_{hv}}{E_h}\delta\sigma_{yy}' \tag{14a}$$

$$E_h = \frac{\delta\sigma_{xx}' - (\nu_{hh} + \nu_{hv})\delta\sigma_{yy}'}{\delta\varepsilon_{xx}} \tag{14b}$$

From undrained conditions, the axis symmetry and Eq. (10b), the following relations are obtained;

$$\delta\varepsilon_{yy} + \delta\varepsilon_{zz} = -\delta\varepsilon_{xx} \tag{15a}$$

$$\nu_{hh} + \nu_{hv} = -\frac{\delta\varepsilon_{yy}}{\delta\varepsilon_{xx}} - \frac{\delta\varepsilon_{zz}}{\delta\varepsilon_{xx}} \tag{15b}$$

$$\nu_{hh} + \nu_{hv} = -\frac{\delta\varepsilon_{yy} + \delta\varepsilon_{zz}}{\delta\varepsilon_{xx}} = -\frac{-\delta\varepsilon_{xx}}{\delta\varepsilon_{xx}} = 1 \qquad (15c)$$

Substitution of Eq.(15c) into Eq.(14b) leads to Young's modulus for the horizontal direction under undrained conditions, $(E_h)_u$.

$$\left(E_h\right)_u = \frac{\delta\sigma_{xx}' - \delta\sigma_{yy}'}{\delta\varepsilon_{xx}} = \frac{\delta q}{\delta\varepsilon_{xx}} \qquad (16)$$

Accordingly, the horizontal Young's modulus is also directly measured from the increment of axial stress and strain from drained or undrained triaxial tests under constant lateral pressure on H-specimens.

Bender Element Tests

In the bender element tests, three kinds of shear moduli (G_{vh}, G_{hh} and G_{hv}) can be calculated from the shear wave velocities from three different directions (V_{vh}, V_{hh} and V_{hv}). Accordingly, all five elastic moduli (Young's and shear moduli) shown in Eq.(2) are obtained from the triaxial loading test and the bender element test.

TEST PROGRAM

Test Material and Sample Preparation Method

The tested material is NSF clay (ρ_s = 2.724 g/cm^3, w_L = 58.4 %, w_P = 28.1 %, IP = 30.3, clay content (< 5 mm) = 100 %). The reconstituted samples were prepared in the laboratory by means of one-dimensional consolidation of slurry having an initial water content of twice the liquid limit. The vertical pre-consolidation pressure was 150 kPa that was maintained constant over 10 days. Specimens with angles between the axial direction of the triaxial specimen and the bedding plain of 0° (V-specimen) and 90° (H-specimen) were cut from the pre-consolidated clay block, as shown in Fig. 1. The diameter and height of specimens are 70 mm and 150 mm, respectively.

Bender Element Tests

In bender element (BE) tests, the shear wave velocities were measured in three different directions (VH, HV, HH-wave). One pair of bender elements was attached to the top cap and the pedestal. Two pairs of bender elements were attached to the lateral surface of the specimen after specimen set up. The lateral BEs were composed of a metallic plate (aluminum plate) glued with one end of a BE (Fioravante 2000). The plate was glued to the internal surface of the membrane with buttonholes (rectangular-hole). The BE was glued on a metal plate through a buttonhole on the membrane using quick-drying glue, after the complete preparation of the specimen (Yamashita et al. 2005). This method does not disturb the specimen, because the BE does not penetrate into the specimen. The transmitting element was driven by ±10V amplitude waves from a generator with a single sinusoidal wave of different frequencies. The effective propagating distance and the arrival time of the shear wave were defined by the distance from tip-to-tip of the bender elements and the starting points of the input and received waves, respectively (Yamashita and Suzuki 2001). The shear wave velocity used was the average of those measured using sinusoidal waves of 10, 15 and 20 kHz.

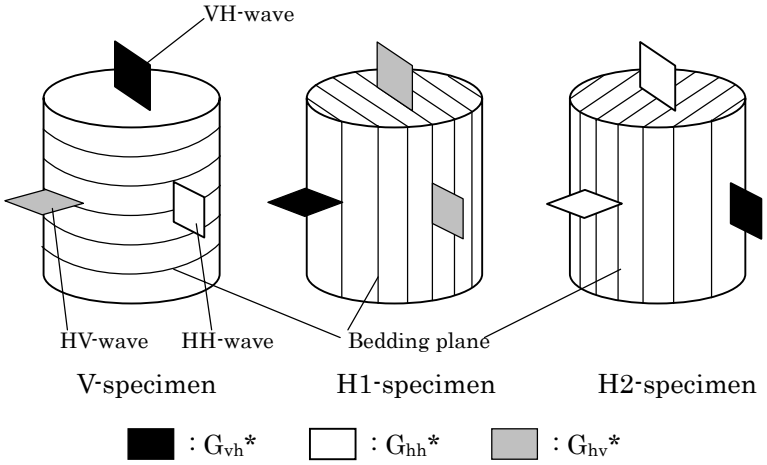

FIG. 2. Relations between Propagating Direction and Bedding Plane

TABLE 1. Relations between Propagating Direction and Shear Moduli

Wave	V-specimen	H1-specimen	H2-specimen
VH-wave	G_{vh}*	G_{hv}*	G_{hh}*
HH-wave	G_{hh}*	G_{hv}*	G_{vh}*
HV-wave	G_{hv}*	G_{vh}*	G_{hh}*

Figure 2 illustrates the relationship of the propagating direction of the shear wave to the bedding plane. There are two kinds of H-specimens based on the difference in penetration direction of the bender elements relative to the bedding plane. The following three kinds of shear moduli ($G = \rho V_S^2$), which were defined by the relations of the propagating direction versus the bedding plane, were measured on these specimens (see Table 1)

G_{vh}* = the propagating direction of the shear wave is perpendicular and the vibrating direction of the particles is parallel relative to the bedding plane;

G_{hh}* = the propagating direction of the shear wave and the vibrating direction of the particles are parallel relative to the bedding plane; and

G_{hv}* = the propagating direction of the shear wave is parallel and the vibrating direction of the particles is perpendicular relative to the bedding plane.

Monotonic and Cyclic Triaxial Tests

After each reconstituted specimen was set up in the cell, the cell pressure was raised to 30 kPa. Subsequently, deaired water was permeated through the specimen. Back pressure of 98 kPa was, thereafter, applied for about one day. All specimens were isotropically consolidated to σ_c' = 49, 98, 196 or 392 kPa. The stress path at consolidation and tested stress states are shown in Fig. 3. The shear wave velocities in three different directions were measured by the bender element (BE) method on each consolidation state (circle mark in Fig. 3 and Table 2). In addition, the undrained equivalent Young's modulus at small strain (0.001 %) was measured by cyclic triaxial (CTX) loading from the same consolidation states. In each state, the

specimen was subjected to eleven undrained loading cycles performed by applying uniform triangular cyclic axial displacements with a frequency of 0.1 Hz. The axial stress and the axial strain were measured by a load cell and one pair of proximity transducers placed inside the cell, respectively. The equivalent Young's modulus, E_{eq}, is defined by the average value of those from the 2nd to 10th cycles. After each specimen was tested with BE and small-strain CTX tests, monotonic undrained triaxial compression (MTX) tests were performed, as shown in Fig. 3 and Table 2.

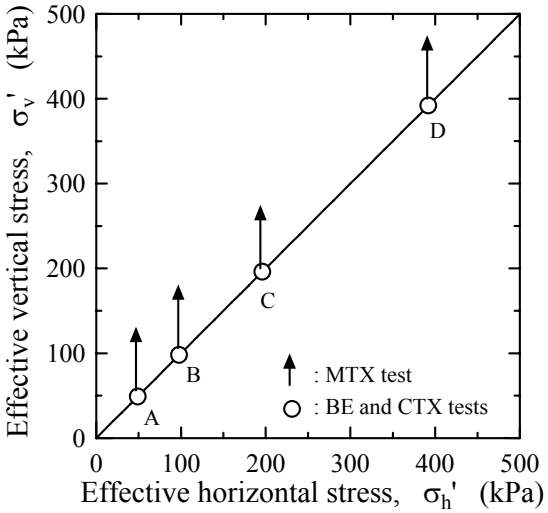

FIG. 3. Stress Path at Consolidation and Tested Stress States

TABLE 2. Test Conditions

Stress points	Effective confining pressure, σ_c'				σ_c' at MTX test
	49 kPa	98 kPa	196 kPa	392 kPa	
	BE, CTX	BE, CTX	BE, CTX	BE, CTX	
A	○	—	—	—	49 kPa
B	○	○	—	—	98 kPa
C	○	○	○	—	196 kPa
D	○	○	○	○	392 kPa

TEST RESULTS

Bender Element Tests

Figure 4 shows some examples of input and received waveforms on V, H1 and H2-specimens in BE tests (σ_c' = 196 kPa, f = 10 kHz). In the V-specimen, the propagation time, Δt, in the HH-wave is clearly faster than that in the HV-wave, as shown in Fig. 4(a). Although Δt in the VH-wave is slower than the others waves because the tip-to-tip distance, Δs, of the bender elements is longer than the others, the shear modulus in the VH-wave, G_{vh}, is similar to G_{hv}. On the other hand, in the H1-specimen, Δt in the HH-wave is almost the same as Δt in the HV-wave, as shown in Fig. 4(b). The shear moduli estimated from the shear wave velocities are almost the same, irrespective of propagating direction in the H1-specimen. Note that in the

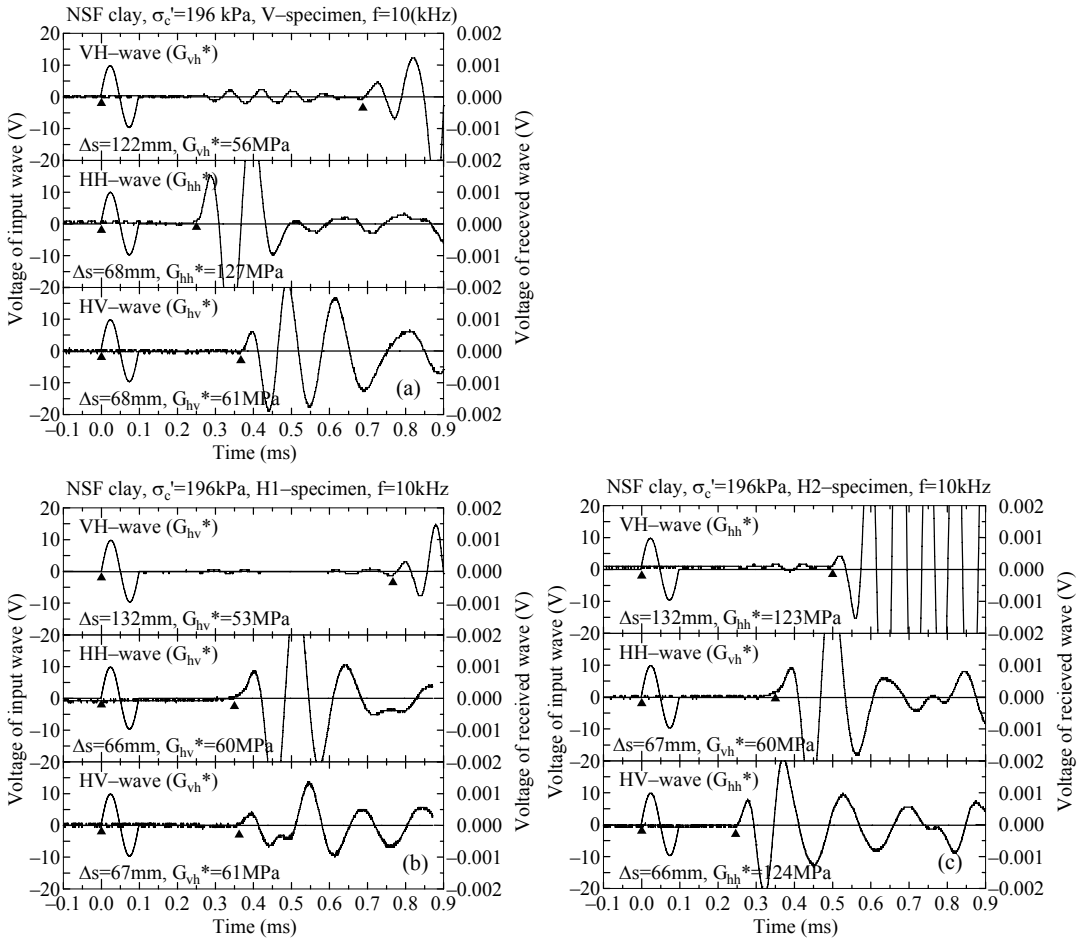

FIG. 4. Examples of input and received waveforms; (a) V-Specimen, (b) H1-Specimen, and (c) H2-Specimen

H1-specimen the propagating or vibrating direction of the shear waves is perpendicular or parallel relative to the bedding plane as shown in Fig. 2. In the H2-specimen, Δt in the HV-wave is faster than that in the HH-wave, as shown in Fig.4(c). Note that in the H2-specimen the propagating and vibrating directions in the HV-wave are both parallel relative to the bedding plane as shown in Fig. 2. Although Δt in the VH-wave is slower than those in the others waves because the tip-to-tip distance, Δs, is longer than the others BEs, the shear modulus in the VH-wave is similar to that in the HV-wave. This is due to the propagating and vibrating directions in VH and HV-waves being both parallel relative to the bedding plane in the H2-specimen, as shown in Fig. 2.

Figure 5 shows the relations of the shear modulus versus the effective confining pressure measured with the same propagating direction of the shear wave relative to the axial direction of the specimen with a different direction of bedding plane. Although the propagating direction of the shear wave relative to the axial direction of the specimen is different, when the propagating direction of the shear wave relative to the direction of bedding plane is the same, the shear moduli for propagation and

vibration parallel to the bedding plane, G_{hh}*, are clearly higher than G_{vh}* and G_{hv}*. G_{vh}* is almost the same as G_{hv}*. From the above discussion, it can be said that shear waves propagate faster in the plane parallel to the bedding plane than perpendicular to it.

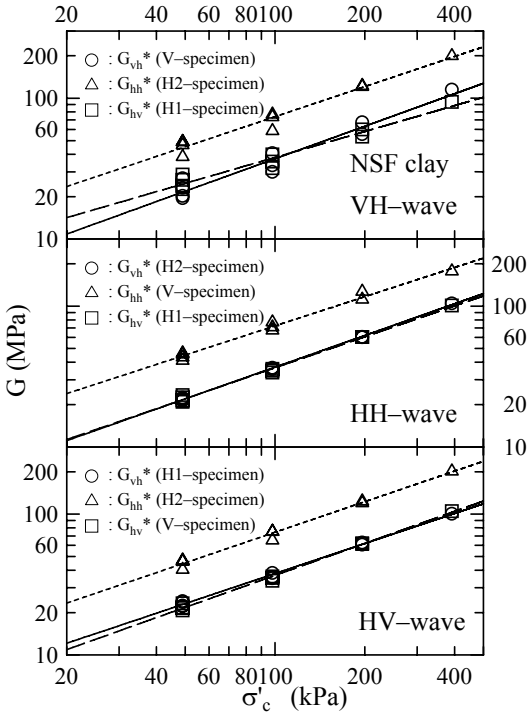

FIG. 5. Effect of Fabric Anisotropy on Shear Modulus

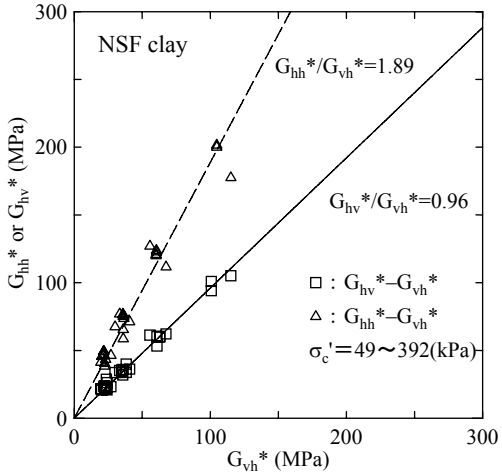

FIG. 6. Relation of G_{hh}* or G_{hv}* to G_{vh}*

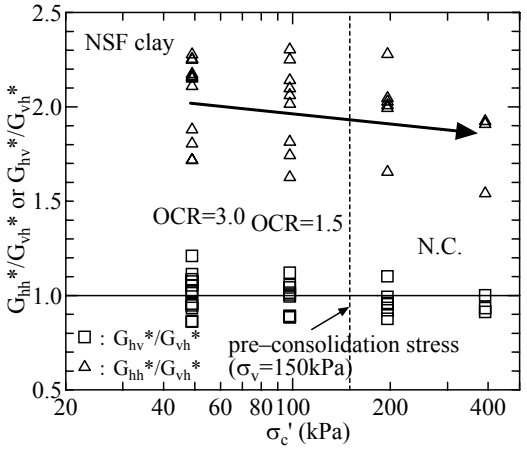

FIG. 7. Relation of Ratio of Shear Modulus to Consolidation Stress

Figure 6 shows G_{hh}* and G_{hv}* versus G_{vh}* on the NSF clay specimens. It can be seen that G_{hh}* is higher than G_{vh}* with an average value of G_{hh}*/(G_{vh}* = G_{hv}*) = 1.9.

This difference of stiffness between G_{hh} and G_{vh} (G_{hv}) is much larger than the results from sand specimens (Yamashita et al. 2005). It would seem that this is because the difference of clay content and mineralogy of soil. The clay content less than 5 micrometer in size of NSF clay is 100 %. The main materials of NSF clay are Quartz and Pyrophyllite from X-ray diffraction. The shape of Pyrophyllite is a plate type.

Figure 7 shows the relation between the ratio of the shear moduli and the confining pressure. It is found that although the horizontal shear modulus, G_{hh}, is larger than the other moduli irrespective of consolidation stress, the ratios of G_{hh} to G_{vh} decrease with an increase of isotropic consolidation stress. It seems that the fabric anisotropy formed by one-dimensional pre-consolidation was decreased by an increase of isotropic confining pressure.

Anisotropy of Elastic Modulus at Small Strain

Figure 8 shows the relationship between the confining pressure and the undrained Young's modulus, $(E)_u$, obtained from undrained MTX and CTX tests at small strains (0.001 %) on V and H-specimens. It is found that the horizontal Young's modulus, E_h (E_{eq} or E_{sec} on H-specimen), is larger than the vertical Young's modulus, E_v (E_{eq} or E_{sec} on V-specimen), irrespective of loading method (monotonic or cyclic).

Figure 9 shows the relation of E_v versus E_h on V and H-specimens. It can be seen that the horizontal Young's modulus, E_h, is much larger than the vertical one, E_v, as well as the shear modulus, and the ratio of E_h/E_v is about 1.5. Figure 10 shows the relation between the ratio of the Young's moduli and the confining pressure. It is also found that the ratios of E_h to E_v decrease with an increase of isotropic confining pressure, as well as the shear modulus. From these results, it is said that the anisotropy of modulus formed by one-dimensional pre-consolidation was decreased by an increase of isotropic confining pressure. Moreover, the anisotropy of stiffness does not disappear, even if the reconstituted sample was consolidated with a doubled pre-consolidation stress.

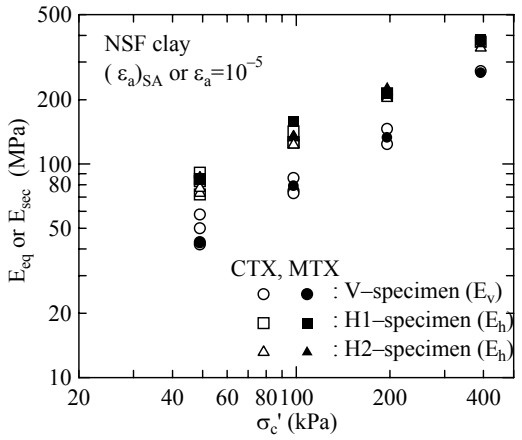

FIG. 8. Young's modulus at small strain Cyclic and Monotonic Triaxial Tests

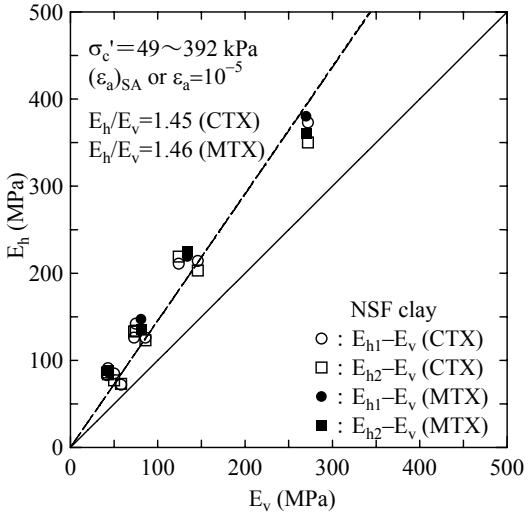

FIG. 9. Relation of E_v to E_h

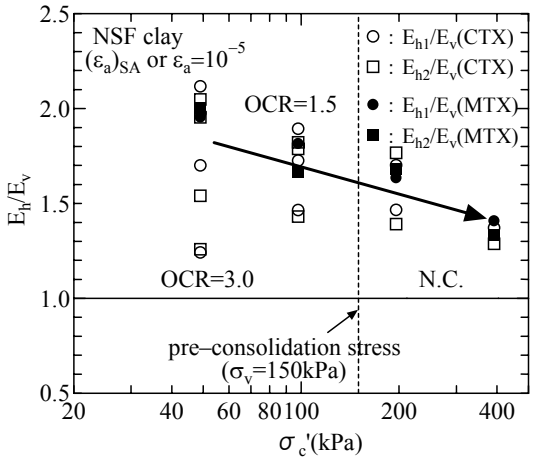

FIG. 10. Relation of Ratio of Young's Modulus to Consolidation Stress

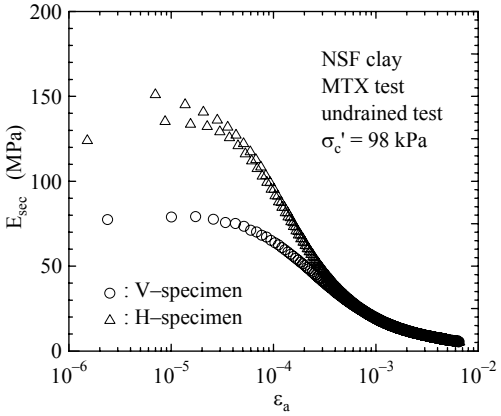

FIG. 11. Young' Modulus at Small to Medium Strains

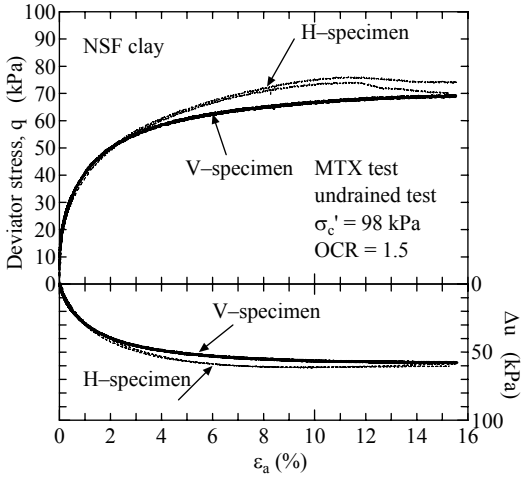

FIG.12. Stress Strain Relation on V and H-specimen

Anisotropy of Elastic Modulus at Small to Large Strains

Figure 11 shows the secant Young's modulus, E_{sec}, plotted against the logarithm of axial strain, ε_a, obtained by monotonic undrained triaxial tests on V and H-specimens. It is found that the Young's modulus on H-specimens is much larger than that on V-specimen at small to medium strains. At strain levels greater than about 5 x 10^{-4}, however, the Young's moduli of V and H-specimens become almost the same. The main reason for this is the lowering of fabric anisotropy induced by the shearing.

Figure 12 shows the stress strain relations of monotonic undrained triaxial compression tests on V and H-specimens up to failure strains. The strength of H-specimens is slightly larger than that of V-specimen at failure due to the difference of excess pore pressure (see Fig. 12). On the other hand, Fig. 13 shows the effective stress paths of undrained MTX tests. Although the maximum deviator stresses of H-specimens are slightly larger than that of V-specimens, the inclinations of deviator and effective confining stresses are almost the same, because the excess pore

pressures of V-specimens are slightly larger than that of H-specimens. This result is the same to the result on reconstituted Kaolin specimens (Duncan and Seed 1966).

Figure 14 shows the ratios of E_h/E_v plotted against the axial strain obtained from monotonic undrained triaxial tests with different consolidation stresses. It is found that the anisotropy of stiffness decreases with an increase of strain levels. The ratios of moduli become unity at an axial strain of about 10^{-2}. The reason seems to be that the disturbance of fabric structure due to the increase of shear stress (strain). However, the ratios become again larger than unity at still larger strain levels due to the difference of excess pore pressure between V and H-specimens, as mentioned above. It is also found that the anisotropy of stiffness decreases with a decrease of consolidation stress.

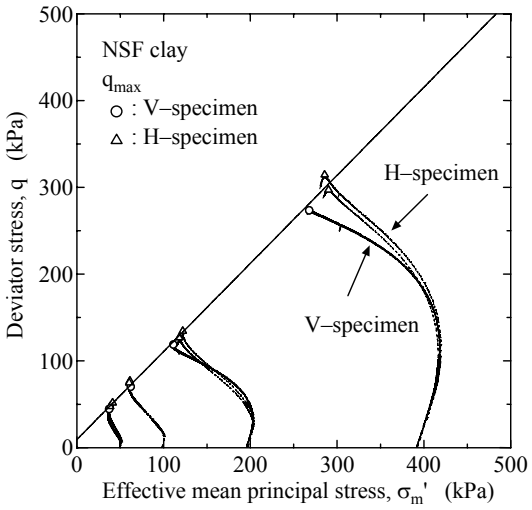

FIG. 13. Effective Stress Path in MTX Test

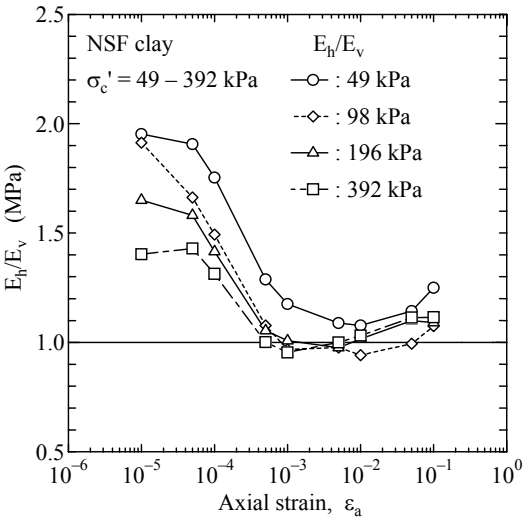

FIG. 14. Relation of Ratio of Young's Modulus to Axial Strain

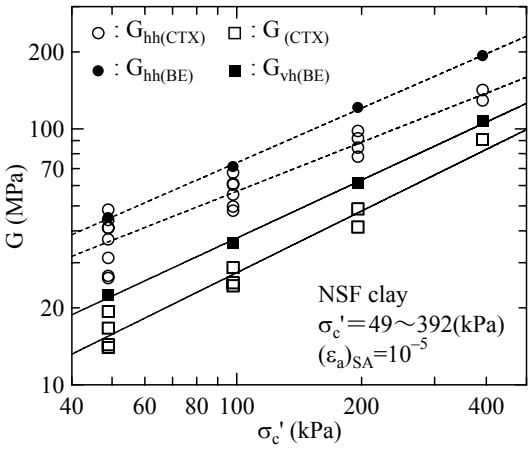

FIG. 15. Comparison of Elastic Modulus by Triaxial and Bender Element Tests

Comparison of Elastic Modulus by Triaxial and Bender Element Tests

Figure 15 shows the comparison between the shear modulus estimated by Young's modulus obtained from undrained triaxial tests and bender element tests. In this figure, the shear moduli from cyclic triaxial tests were estimated using two methods. One method assumed that the specimen was an isotropic homogeneous elastic medium, and the shear modulus was estimated from the result of CTX test;

$$G_{(CTX)} = \frac{E_v}{2(1+\nu_u)} \tag{17}$$

where E_v is the Young's modulus of V-specimen; ν_u is the undrained Poisson's Ratio ($\nu_u = 0.5$).

Another method is using the cross-anisotropic elastic model;

$$G_{hh(CTX)} = \frac{E_h}{2(1+\nu_{hh})} \tag{7 bis}$$

where E_h is the Young's modulus of H-specimen; ν_{hh} is obtained from the following relations;

$$\frac{E_h}{E_v} = \frac{\nu_{hv}}{\nu_{vh}} = \frac{\nu_{hv}}{0.5} \tag{6 bis}$$

$$\nu_{hh} + \nu_{hv} = 1 \tag{15c bis}$$

where ν_{hv} was the estimated by the ratio of E_h/E_v in triaxial tests.

From Fig. 15, the shear modulus, assumed as an cross-anisotropic specimen, $G_{hh(CTX)}$, and obtained from BE tests, $G_{vh(BE)}$ and $G_{hh(BE)}$, are larger than that assumed as an isotropic homogeneous specimen, $G_{(CTX)}$. It is also found that the horizontal shear modulus obtained from CTX tests, $G_{hh(CTX)}$, is smaller than that from BE tests, $G_{hh(BE)}$. This reason seems to be that the effects of the difference of strain level in CTX (10^{-5}) and BE ($<10^{-5}$) tests, the bedding error in triaxial tests, and the low B-value in the undrained triaxial tests (B was about 0.9), etc. Thus, for example, the assumption of an undrained Poisson's Ratio, ν_u, of 0.5 might be incorrect. Further research will be necessary to clarify the difference between the results of triaxial and bender element tests. However, it is concluded at least that the shear modulus estimated from triaxial test using the isotropic elastic model underestimates the modulus.

In this study, the tested clay is only kind of clay. The sample is artificially created from a one-dimensional pre-consolidation sample. As a result, the anisotropy of stiffness might be larger. Further research will be necessary using the others kinds of clays and undisturbed samples.

CONCLUSIONS

(1) The G_{vh} is almost the same to the G_{hv} on NSF clay samples as well as sand samples. On the other hand, the G_{hh} is much larger than the G_{vh} and G_{hv} on reconstituted NSF clay samples under isotropic consolidated state.
(2) The E_h at small strains is also larger than the E_v on reconstituted NSF clay sample under isotropic consolidated state.
(3) The anisotropy of stiffness on NSF clay is larger than the results on sand

specimens. The reasons seem the difference of clay content, clay mineral.

(4) The anisotropy of stiffness at small strain becomes lower with the increase in strain level and consolidation stress.

(5) The shear modulus estimated from the E_v on CTX tests is lower than that from BE test.

REFERENCES

Butcher, A.P. and Powell, J.M.M. (1995). "The effects of geological history on the dynamic stiffness in soils." *Proc. 11th European Conf. on Soil Mechanics*, Copenhagen, 1, 127-136.

Dumcan, J. M. and Seed, H. B. (1966). "Anisotropy and stress reorientation in clay." *Journal of the Soil Mechanics and Foundation*, ASCE, 92(SM5), 21-50.

Dyvik, R. and Madshus, C. (1985). "Laboratory measurement of Gmax using bender elements." *Advances in the Art of Testing Soils under Cyclic Conditions; Proc. a session sponsored by the Geotechnical Engineering Division in conjunction with the ASCE Convention*, Detroit, ASCE, 1, 186-196.

Fioravante, V. (2000). "Anisotropy of small strain stiffness of Ticino and Kenya sands from seismic wave propagation measured in triaxial testing." *Soils and Foundations*, JGS, 40(4), 129-142.

Hight, D.W., Bennell, J.D., Chana, B., Davis, P.D., Jardine, R.J. and Provic, E. (1997). "Wave velocity and stiffness measurements of the Crag and Lower London Tertiaries at Sizewell." *Géotechnique*, ICE, 47(3), 451-474.

Yamashita, S., Hori, T. and Suzuki, T. (2005). "Effects of initial and induced anisotropy on initial stiffness of sand by triaxial and bender elements test." *Geomechnics*, *Testing*, *Modeling*, *and Simulation*, J. A. Yamamuro and J. Koseki, eds., ASCE, GSP No.143, 350-369.

Yamashita, S. and Suzuki, T. (2001). "Small strain stiffness on anisotropic consolidated state of sands by bender elements and cyclic loading tests." *Proc. of 15th ICSMGE*, Istanbul, 1, 325-328.

Yimsiri.,S. and Soga,K. (2002). "Application of micromechanics model to study anisotropy of soils at small strains." *Soils and Foundations*, JGS, 42(5), 15-26.